Available online at www.sciencedirect.com

ScienceDirect

Scripta Materialia 83 (2014) 13–16

Scripta MATERIALIA

www.elsevier.com/locate/scriptamat

# Intrinsic point defects in thermoelectric half-Heusler alloys

Yaw Wang Chai,[a,b,*] Kentaro Yoshioka[b] and Yoshisato Kimura[b]

[a] *ALCA-Japan Science and Technology Agency, 4-1-8 Honcho, Kawaguchi-shi, Saitama 332-0012, Japan*

[b] *Department of Materials Science, Interdisciplinary Graduate School of Science and Engineering, Tokyo Institute of Technology, and Engineering, 4259-J3-19 Nagatsuta, Midori-ku, Yokohama 226-8502, Japan*

Received 26 February 2014; revised 28 March 2014; accepted 29 March 2014
Available online 5 April 2014

The single-phase half-Heusler microstructure of ZrNiSn, ($Zr_{0.5}$, $Hf_{0.5}$)NiSn and Zr(Ni, $Co_{0.2}$)Sn alloys was found to contain a high density of Heusler lattice bands 2–7 nm wide. These nanoscale Heusler lattice bands originated from clustering of Ni and/or Co antisites via occupation of structural vacancies by excess Ni or (Ni+Co) concentrations. The presence of these lattice point defects and their subsequent clustering could result in the reduction of thermal conductivity of the half-Heusler alloys.


*Keywords:* Half-Heusler alloys; Nanoscale Heusler bands; Lattice point defects; Lattice strain; Thermal conductivity

The thermoelectric properties of half-Heusler (HH) semiconductor compounds are closely related to their electronic structure, which in turn is sensitive to deviation from stoichiometric composition. The current study is aimed at investigating microstructural changes, particularly generation of lattice point defects, which often results from the deviation of HH stoichiometric composition. Point defects in HH alloys have been reported to reduce thermal conductivity (κ) and band gap ($E_g$), alter electrical transport and possibly even induce half-metallicity [1–7]. Many have reported a variety of point defects in XYSn (X = Ti, Zr, Hf; Y = Ni, Co) HH alloys, including Ni antisites (where Ni occupies structural vacancies) [8], X–Sn swap disorders [1] and vacancies [6]; Ni antisites have been found to be the most energetically favorable [2,8,9]. In our previous studies [10,11], we showed in HH alloys that Ni antisites tend to cluster, forming Heusler (H) phase nanoprecipitates containing slight excesses of Ni. However, subsequent investigations suggested that the antisite clustering, prior to inducing the Heusler nanoprecipitation, might generate an intermediate nanoscale microstructure. The effect of the nanoscale microstructure will also be discussed mainly in conjunction with the κ of the alloys determined previously by Kimura et al. [12,13].

HH ($C1_b$-type) and H ($L2_1$-type) crystal structures are formed by four interpenetrating face-centered cubic (fcc) sublattices located at I-(0, 0, 0), II-(1/4, 1/4, 1/4), III-(1/2, 1/2, 1/2) and IV-(3/4, 3/4, 3/4)—see Fig. 1 in Ref. [11]. In both XYSn HH and $XY_2Sn$ H alloys, sublattices I and III are occupied by X and Sn atoms, respectively, forming an energetically stable NaCl substructure. The HH structure becomes more stable when either the II or IV sublattice is occupied by Ni atoms while the other is vacant [1,8]. In the current paper we refer to the vacant site of the HH structure as a structural vacancy (SV) to avoid confusion with vacancy point defects. In the H structure, both the II and IV sublattices are occupied by Ni atoms. The HH and H structures can be distinguished by their $\{111\}_{HH}$ lattice structure, as demonstrated in our previous study [10].

We chose three alloys for the current study: ZrNiSn, ($Zr_{0.5}$, $Hf_{0.5}$)NiSn and Zr(Ni, $Co_{0.2}$)Sn. A previous study found that, in the Zr(Ni, $Co_{0.2}$)Sn alloy, the additional Co atoms preferentially occupied the SVs of the HH structure [12]; we define these point defects as Co antisites. The alloys were prepared by arc melting, followed by directional solidification by using optical floating zone melting. Alloys prepared by this method have grain sizes well over 300 μm. The phase identity on microstructure

* Corresponding author at: Department of Materials Science, Interdisciplinary Graduate School of Science and Engineering, Tokyo Institute of Technology, and Engineering, 4259-J3-19 Nagatsuta, Midori-ku, Yokohama 226-8502, Japan. Tel.: +81 (0)45 924 5495; e-mail addresses: chai.y.aa@m.titech.ac.jp; yawwangchai@gmail.com

http://dx.doi.org/10.1016/j.scriptamat.2014.03.025
1359-6462/

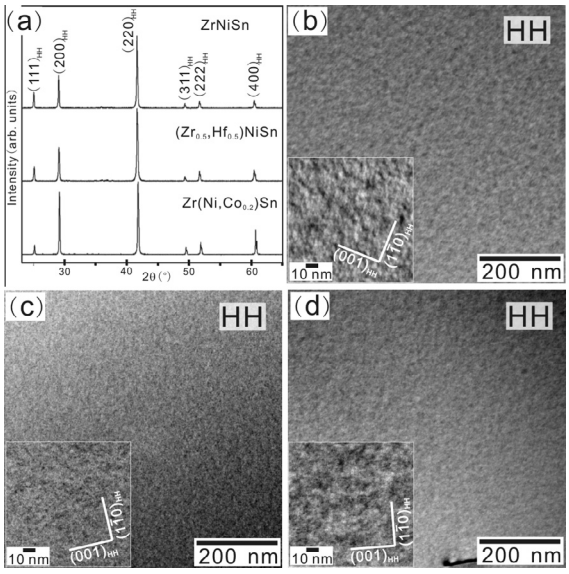


**Fig. 1.** (a) XRD profiles indicate the ZrNiSn, ($Zr_{0.5}$, $Hf_{0.5}$)NiSn and Zr(Ni, $Co_{0.2}$)Sn alloys, are nearly single HH phase. Bright-field TEM images reveals the modulated-like HH microstructure in the (b) ZrNiSn, (c) ($Zr_{0.5}$, $Hf_{0.5}$)NiSn, and (d) Zr(Ni, $Co_{0.2}$)Sn alloys. The enlarged images in the insets reveal the modulated structures.

of the alloys was determined by X-ray diffraction (XRD). In the current paper, the compositions of these alloys were analyzed by electron-probe microanalysis (EPMA), and their microstructures were characterized by using transmission electron microscopy (TEM) and high-resolution TEM (HRTEM) at 200 kV. Our TEM specimen preparation has been described elsewhere [11].

Composition analyses by EPMA have found that the alloys are HH phase with slight deviations from stoichiometric compositions, $Zr_{0.95}Ni_{1.09}Sn$, ($Zr_{0.5}$, $Hf_{0.5}$)$_{0.91}Ni_{1.09}Sn$ and $Zr_{0.95}$(Ni, $Co_{0.16}$)Sn (see Table 1). Note the trend in composition deviation: the Zr and (Zr+Hf) concentrations were often slightly lower than the stoichiometric value (i.e. molar ratio $< 1$) and accordingly the Ni and (Ni+Co) concentrations were slightly higher (i.e. molar ratio $> 1$). Because of the additional Co in the Zr(Ni, $Co_{0.2}$)Sn alloy, we expected the (Ni+Co) molar ratio to be >1. Similar trends in compositional deviations have been noted in HH alloys fabricated with other techniques (e.g. levitation melting) [14]. The XRD profiles in Figure 1a have further confirmed that the three alloys, ZrNiSn, ($Zr_{0.5}$, $Hf_{0.5}$)NiSn and Zr(Ni, $Co_{0.2}$)Sn alloys, are single HH phase. Nevertheless, detection of any microstructural changes in these alloys induced by the subtle deviation from HH stoichiometric composition was rather difficult using XRD and scanning electron microscopy. In contrast, using TEM we did observe microstructural changes, as shown in Figure 1.

Bright-field TEM images in Figure 1b–d show the HH microstructure of the ZrNiSn, ($Zr_{0.5}$, $Hf_{0.5}$)NiSn and Zr(Ni, $Co_{0.2}$)Sn alloys, respectively. Their microstructure was found to contain a high density of strain contrast that resembled a "modulated"-like structure with a very small spacing (<10 nm). Using HRTEM, it was found that the modulated structure originated from lattice distortions throughout the HH matrix, as shown in Figure 2a–c. These lattice distortions also contributed to splitting of the diffraction spots in the corresponding $[110]_{HH}$ fast Fourier transform (FFT) patterns; these distortions are indicated by arrows in the insets of the enlarged diffraction spots in Figure 2a–c. This behavior implies that the lattice distortions must be caused by localized variation of lattice sizes within the HH matrix. To further analyze the distorted lattice structure, we performed inverse FFT (IFFT) image processing, as shown in Figure 2d–f. These IFFT images reveal that the lattice distortions are not randomly distributed, but rather are "grouped" together, forming networks of small distorted lattice bands, 2–7 nm wide, throughout the HH matrix. The nanoscale bands are coherent with the surrounding HH matrix, exhibit no preferred orientation and have widths that do not vary appreciably across the three alloys. However, the spacing between the nanoscale distorted lattice bands appears to be larger in the ZrNiSn and ($Zr_{0.5}$, $Hf_{0.5}$)NiSn alloys (~7 and ~8 nm, respectively) than in the Zr(Ni, $Co_{0.2}$)Sn alloy (~5 nm), indicating in the latter a larger volume fraction of bands.

Figure 3a–c show sections of the IFFT images, which consist of the distorted and HH lattices. The structures of the distorted lattice bands are i, iii and v, while the corresponding HH lattice structures are ii, iv and vi. By analyzing the i, iii and v configurations, we found they most resembled the lattices of H-phase structures. This result suggests that the SVs in the supposed HH structure are occupied, most likely by excess Ni atoms in the ZrNiSn and ($Zr_{0.5}$, $Hf_{0.5}$)NiSn alloys, forming Ni antisites as shown schematically in Figure 3a and b, and excess Ni and Co atoms in the Zr(Ni, $Co_{0.2}$)Sn alloy, forming Ni and Co antisites as shown schematically in Figure 3c. We only considered Ni point defects and Co antisites here because their formations were more energetically favorable than other point defects [2,3,8,9]. Figures 1–3 further suggest clustering in the HH matrix of Ni and/or Co antisites, forming the larger H-lattice bands. The coexistence of nanoscale H-lattice bands and the HH matrix also suggests that the HH and H phases lack mutual solubility, in agreement with predictions by Kirievsky et al. [9]. Although these

**Table 1.** Composition analyses of the HH alloys by EPMA.

| Nominal composition | Chemical composition (at.%) | | | | | Molar ratio |
|---|---|---|---|---|---|---|
| | Zr | Hf | Ni | Co | Sn | |
| ZrNiSn | 31.2 | – | 35.9 | – | 32.9 | Zr:Ni:Sn = 0.95:1.09:1 |
| ($Zr_{0.5}$,$Hf_{0.5}$)NiSn | 15.4 | 15.0 | 36.3 | – | 33.3 | (Zr+Hf):Ni:Sn = 0.91:1.09:1 |
| Zr(Ni,$Co_{0.2}$)Sn | 30.5 | – | 32.2 | 5.2 | 32.1 | Zr:(Ni+Co):Sn = 0.95:1.17:1 |